Distinct oxygen hole doping in different layers of $Sr_2CuO_{4-\delta}/La_2CuO_4$ superlattices

S. Smadici,[1] J. C. T. Lee,[1] A. Rusydi,[2] G. Logvenov,[3,*] I. Bozovic,[3] and P. Abbamonte[1]
[1]*Frederick Seitz Materials Research Laboratory, University of Illinois, Urbana, Illinois 61801, USA*
[2]*NUSSNI-NanoCore, Department of Physics, National University of Singapore, 117542, Singapore*
[3]*Brookhaven National Laboratory, Upton, New York 11973, USA*
(Received 10 November 2011; revised manuscript received 30 January 2012; published 28 March 2012)

X-ray absorption in $Sr_2CuO_{4-\delta}/La_2CuO_4$ (SCO/LCO) superlattices shows a variable occupation with doping of a hole state different from holes doped for $x \lesssim x_{\text{optimal}}$ in bulk $La_{2-x}Sr_xCuO_4$ and suggests that this hole state is on apical oxygen atoms and polarized in the a-b plane. Considering the surface reflectivity gives a good qualitative description of the line shapes of resonant soft x-ray scattering. The interference between superlattice and surface reflections was used to distinguish between scatterers in the SCO and the LCO layers, with the two hole states maximized in different layers of the superlattice.

DOI: 10.1103/PhysRevB.85.094519 PACS number(s): 74.78.Fk

I. INTRODUCTION

Hole doping of $La_{2-x}Sr_xCuO_4$ is described in the Zhang-Rice singlet (ZRS) upper Hubbard band (UHB) model for $0 < x \lesssim 0.2$ as ZRS states on in-plane oxygen atoms. These holes are visible as a feature in x-ray absorption spectroscopy (XAS) at the O K edge, called the mobile carrier peak (MCP). The MCP gains intensity with doping at the expense of LHB (lower Hubbard band) states and concurrent "spectral weight transfer" from UHB states. This model, expanding the Cu $d_{x^2-y^2}$ one-band Mott-Hubbard model to the Cu $d_{x^2-y^2}$, O p_x, O p_y three bands of the CuO_2 planes, describes well the variation, observed with XAS at the O K edge of unoccupied density of states in cuprates for relatively low doping ($x \lesssim 0.2$).[1,2]

However, the variation of the maximum critical temperature $T_{c,\max}$ between different superconducting compounds can not be explained within the UHB-ZRS model and its in-plane orbitals only, and possible extensions of the model to out-of-plane orbitals have been intensively investigated. Since there can be only one Fermi surface for an isolated CuO_2 plane, other indications of the relevance of out-of-plane orbitals came from angle-resolved photoemission (ARPES) measurements of square- and diamond-shaped Fermi surfaces for La_2CuO_4 (Ref. 3) and $Ca_2CuO_2Cl_2$ (Ref. 4). The most relevant out-of-plane orbital that hybridizes with states in the CuO_2 plane is the apical oxygen p_z orbital mixed with the Cu $3d_{3z^2-r^2}$ (Refs. 5 and 6) or 4s (Ref. 7) orbital in the CuO_2 planes. The occupation of the apical oxygen orbitals modifies the bond valence sums and was used to explain general trends of $T_{c,\max}$.[8,9] The effect of apical oxygen p_z energy level on parameters of an expanded t-J model has been considered for different materials.[10] In contrast, the axial hybrid between the O p_z and Cu 4s orbitals, with Cu$d_{3z^2-r^2}$ states occupied, has been addressed in Ref. 7. These calculations predicted that an empty apical oxygen p_z orbital modifies the in-plane hole hopping parameter t' between sites along the orthorhombic axes, consistent with ARPES measurements, with a suppressed t' from the presence of unoccupied apical oxygen orbitals correlating with a smaller $T_{c,\max}$.[7,10,11]

In addition, the depletion of the UHB states in bulk $La_{2-x}Sr_xCuO_4$ at $x \sim 0.2$ (Ref. 2) shows that the ZRS-UHB model also needs to be modified to describe the hole doping for higher x. However, because of limits of bulk crystal growth, doping dependence studies have been limited to doping near $x = 2$, realized in bulk $Sr_2CuO_{4-\delta}$ with a very large T_c,[12–18] where the oxygen atoms are removed from the structure ($\delta > 0$), and for relatively low x, near the superconducting dome, where there is evidence of a qualitative change with x in the doping process near x_{optimal}. Specifically, the effective Cu ion magnetic moment in $La_{2-x}Sr_xCuO_4$ and the magnetic exchange between Cu spins are strongly reduced[19] at $x \sim 0.2$ and the T-independent Pauli paramagnetism is replaced at $x \sim 0.22$ by T-dependent Curie paramagnetism with increased doping.[20] Calculations[5,6] suggested that the doping mechanism is different for $x > x_{\text{optimal}}$, as the number of a_1-symmetry states, related to the Cu $3d_{3z^2-r^2}$ orbital[10] and exceeding the optimal doping x_{optimal}, correlated with $T_{c,\max}$. A small but growing contribution from apical oxygen p_z orbital holes mixed with Cu $d_{3z^2-r^2}$ orbitals at MCP was inferred from angle-resolved XAS measurements[21] and from the variation of the Cu-apical oxygen distance with doping,[22] which also correlates with a variation in T_c.[23,24] Recently, a saturation of the XAS MCP intensity with increasing doping near x_{optimal} was observed,[25] and dynamical mean-field theory calculations[26] concluded that either additional orbitals become relevant in this doping range or that new model parameters would be needed to account for multiple-hole interactions. The additional orbital or band to consider in the $La_{2-x}Sr_xCuO_4$ hole doping process between $x \sim 0.2$ and 2 is not known.

In this study, doping in the range $1 \lesssim x \lesssim 1.5$, inaccessible with bulk crystal growth techniques, was obtained with $Sr_2CuO_{4-\delta}/La_2CuO_4$ (SCO/LCO) superlattice (SL) growth. We observed that occupations of two distinct oxygen hole states are gradually modified with doping. By using the interference of the SL reflections with the surface reflection, we determined that the two hole states are maximized in different layers. This suggests that the states emptied preferentially in the SCO layers are the additional states in the extension of the ZRS-UHB model to this doping range.

II. EXPERIMENTS

A. Superlattice structure

The superlattice samples were grown by molecular beam epitaxy on $LaSrAlO_4$ (LSAO) substrates at Brookhaven

National Laboratory. From $a_{SCO} = 3.765$ Å (Ref. 27), $a_{LCO} = 3.810$ Å (Ref. 28), and $a_{LSAO} = 3.756$ Å (Ref. 23), the in-plane lattice mismatch between SCO and LCO layers and substrate is 0.25% and 1.5%, respectively. During growth, the substrate temperature was approximately 750 °C and the O_2/O_3 pressure was approximately 8.5×10^{-6} Torr. The growth was monitored with reflection high-energy electron diffraction (RHEED). After growth, the samples were cooled to 500 °C, followed by pumping down to 10^{-7} Torr and cooling to room temperature. For more details on oxide molecular beam epitaxy, see Refs. 29 and 30. The samples were stored in a dehumidified environment, with exposure to air minimized to a few minutes before resonant soft x-ray scattering (RSXS) measurements, and a few hours during hard x-ray diffraction (HXD) measurements.

Three SL, called SL-A, SL-B, and SL-C in the following, were chosen after atomic force microscopy (AFM) and HXD measurements. HXD measurements [Fig. 1(b)] were made using a Philips X′ Pert diffractometer. From a Nelson-Riley fitting, the number of layers in one superperiod for SL-A and SL-C is $N = 7.81 \pm 0.1$ ML and $N = 9.27 \pm 0.3$ ML, respectively, where 1 ML ("molecular layer") is the average d spacing of one SL "formula-unit" layer (half the unit cell), given by the (002) reflection. The SL structure was further characterized with RSXS measurements at beamline X1B at the National Synchrotron Light Source. Reflectivity measurements near the La edge [Fig. 1(c)] for $Q = (0,0,Q_z)$, where $Q_z = 2\pi L/c_{SL}$ is the scattering momentum in units of SL superperiod c_{SL}, show superperiods with an integer number of layers, $N = 8$ and 9 ML for SL-A and SL-C, respectively, consistent with the HXD measurements. The slightly worse SL-B has $N = 7.8$ ML. The thickness of the SCO layers within a SL superperiod is $N_{SCO} \approx 2$ ML for all samples, but somewhat larger for SL-A compared to SL-B or SL-C because of larger doping (Sec. II B). The number of repeats was 8, 7, and 8 for SL-A, SL-B, and SL-C, respectively. The total SL thickness from RHEED oscillations (not shown), hard x-ray thickness oscillations [Fig. 1(b)], and RSXS measurements [Fig. 1(c)] was 480 ± 50 Å, 480 ± 80 Å, and 520 ± 40 Å for SL-A, SL-B, and SL-C, respectively. A sketch of one SL superperiod is shown in Fig. 1(a) (inset).

The superconducting critical temperatures from ac susceptibility measurements were 25 K for SL-A, 38/39.5 K for for SL-B, and 14/36.5 K for SL-C, where the first and second values for SL-B and SL-C are for measurements before and after ozone annealing at 350 °C for 20 min [Fig. 1(a)]. AFM images were taken on a Dimension 3100 instrument. They showed a surface covered by islands approximately 150 nm wide and 2 nm high for SL-B (data not shown); SL-A or SL-C did not have these features. The AFM surface RMS roughnesses σ_s for SL-A, SL-B, and SL-C were 0.61, 0.76, and 0.43 nm, respectively.

The interface roughness can be characterized with HXD reflectivity. The $L = 1$ reflection width [Fig. 1(b)], dominated by the total SL thickness and not sufficiently sensitive to small-scale roughness, was approximately the same for all SL. However, the $L = 2$ linewidth was the same for SL-A and SL-C and 9% higher for SL-B. Also, the $I(L = 2)/I(L = 1)$ ratio was the same for SL-A and SL-C and 23% smaller for SL-B. These observations suggest that SL-A or SL-C have a

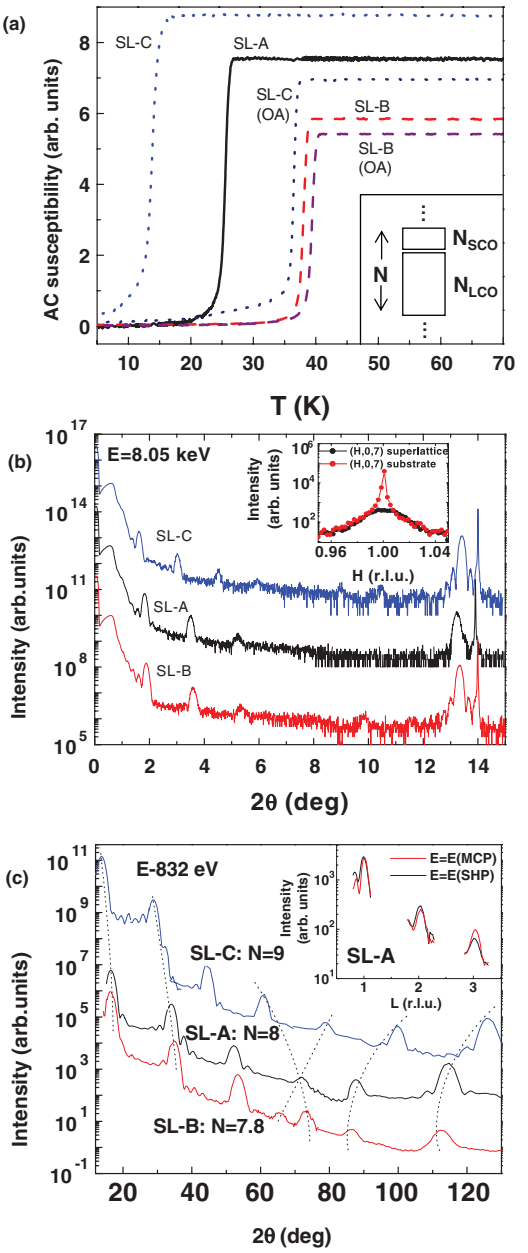

FIG. 1. (Color online) (a) Measurements before and after ozone annealing (OA) show that all SL are superconducting. The inset shows a sketch of one SL superperiod. The atomic planes within the SCO and LCO layers are shown in Fig. 6(a). (b) Hard x-ray reflectivity characterization ($E = 8.05$ keV). The sharp peak at $2\theta \approx 14°$ is the substrate (002) reflection peak, with $c_{LSAO} = 12.64$ Å (Ref. 23). Using this peak as a reference marker, HXD measurements showed that the average ML thickness was 6.64, 6.63, and 6.59 Å for SL-A, SL-B, and SL-C, respectively. The difference is consistent with the thicknesses of the SCO and LCO layers in each SL and the larger c-axis parameter of SCO films $c_{SCO} = 13.55$ Å (Ref. 24) compared to that of LCO films $c_{LCO} = 13.3$ Å. Superlattices with smaller LCO layer thickness in a superperiod (not shown) had less good growth. The inset shows the epitaxial growth, where $a_{LSAO} = 3.76$ Å (Ref. 23). (c) Characterization with soft x rays near the La edge ($E = 832$ eV). The dotted lines show the evolution of the SL peaks with superperiod thickness (Ref. 31). Inset shows L scans at MCP and SHP energies (Sec. II D). The difference at $L = 3$ between MCP and SHP amplitudes is also visible in Fig. 4.

smaller interface roughness σ_i than SL-B, consistent with the AFM and superperiod measurements. In addition, although the surface roughness σ_s of SL-A is larger than that of SL-C, their interface roughnesses σ_i are similar. This will be used to explain the difference in scattering at the O edge between SL-A and SL-C (Sec. III B).

For an estimate of the Sr doping range, we use a SL interface RMS roughness $\sigma_i \sim 6$ Å from estimates based on AFM, HXD, and RSXS measurements. The maximum Sr doping is estimated with either a "flat-top" or a Poisson distribution as $x_{\max} \sim 1.5$ and $x_{\max} \sim 1$ for a SL with 3-ML and 2-ML thick SCO layers, respectively, outside the current possibilities of bulk crystal growth. Therefore, the middle nominally SCO layer in a 3-ML-thick SCO layer is approximately $La_{0.5}Sr_{1.5}CuO_4$ and the two nominally SCO layers in a 2-ML-thick SCO layer are approximately $LaSrCuO_4$. The shorthand notation "SCO" and "LCO" from the deposition sequence will continue to be used for simplicity for the SL layers. Our conclusions do not depend on the exact values of SCO and LCO layer thickness or interface roughness.

B. Oxygen edge fluorescence yield

The first indication of hole doping at two distinct energies comes from XAS measurements with fluorescence yield (FY) detection and π-polarized incident light, made at beamline X1B with a spherical grating monochromator at the National Synchrotron Light Source. A similar instrument is described in Ref. 32. For FY measurements, the entrance slit was 70 μm and the exit slit was 100 μm, with a calculated energy resolution of 0.39, 0.43, and 1.23 eV at 520, 550, and 930 eV, respectively. The typical step size was 0.25 eV, with typical count times of 10 seconds for each point. The sample and detector angles were $\theta = 80^\circ$ and $2\theta = 110^\circ$, respectively, defined as shown in Fig. 2(b) (inset). Calculated soft x-ray absorption depths are considerably larger than the SL total thickness (Sec. II A); for instance, the absorption depths are 1900, 1450, and 1550 Å in LCO at the O K, La M, and Cu L edges, respectively.

In FY spectroscopy, an electron from a core state is excited to an unoccupied state. As the electron returns to the core state, fluorescence radiation is emitted that, for a grazing outgoing beam, is proportional to the x-ray absorption probability. In the simplest model, the x-ray absorption probability is proportional to the density of unoccupied states. In general, because of different Coulomb and exchange interactions in the ground and excited states, this is not the case. However, these atomic multiplet effects are small at the O K edge. For a quantitative analysis of FY line shapes of crystalline solids, crystal field and charge-transfer effects need also to be considered.[33] In comparing the FY results on different SL, we discuss the FY line shapes qualitatively.

SL measurements are shown in Fig. 2(a). FY of bulk $La_{2-x}Sr_xCuO_4$ (LSCO) has three main low-energy features[2]: the MCP of the ZRS state, the UHB feature, and a peak called here the "second hole peak" (SHP). The highest peak at 536.1 eV, sometimes associated with orbitals mixed with La states,[34] is followed by "continuum oscillations." There is no clearly discernible UHB peak in SL FY. The UHB intensity in bulk LSCO is negligible[2] for $x > 0.15$; therefore,

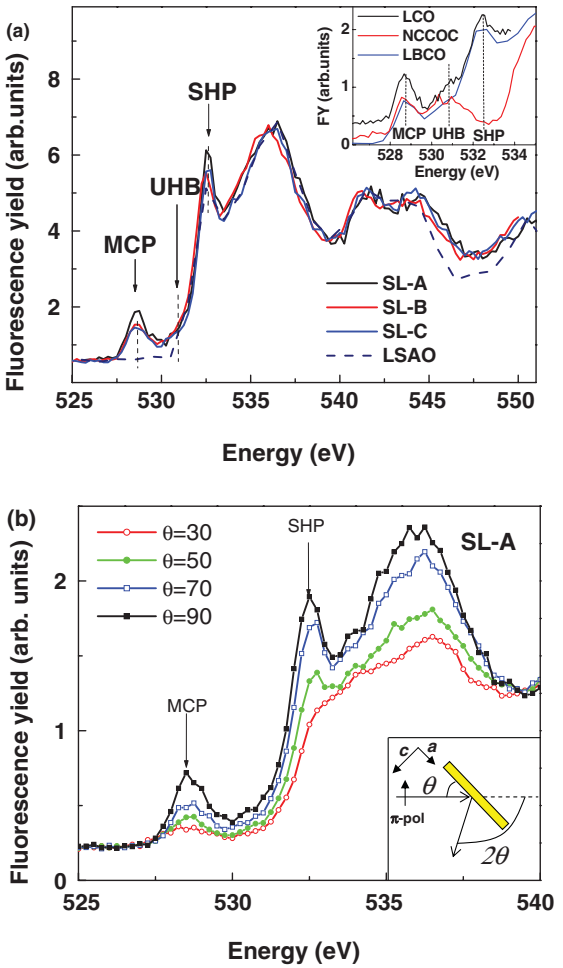

FIG. 2. (Color online) (a) Superlattice fluorescence yields differ at the MCP and SHP energies only. The relative intensities of the MCP peaks in fluorescence yield make it clear that SL-A has more Sr than SL-B and SL-C. Since the LSAO substrate SHP is smaller than that of either SL, sampling more substrate FY in SL-A measurements (SL-A is thinner than SL-C) can not explain the higher SHP intensity. The inset shows for comparison FY for bulk $La_{2-x}Ba_xCuO_4$ (with $x = 0.125$), $La_2CuO_{4+\delta}$ (with $\delta = 0.12$), and $Na_xCa_{2-x}CuO_2Cl_2$ (NCCOC with $x = 0.08$). The energy was calibrated by aligning MCP at 528.5 eV or, when this peak was not present, by aligning at SHP. (b) Angle-resolved fluorescence yield on SL-A. The measurements have been aligned at 525 and 560 eV. Inset shows the measurement geometry. The detector angle 2θ was kept fixed at 110°.

the nominally undoped LCO layers in the SL are instead thoroughly doped with MCP holes (the occupation factor $\langle t_{l,\mathrm{LCO}}^{\mathrm{MCP}} \rangle > 0.15$), consistent with estimates based on roughness and hole diffusion length.[35]

The measured SL FY_{measured} spectra have been aligned in Fig. 2(a) at two energies E_1 and E_2 (below and above the edge), with the linear transformation $\mathrm{FY}_{\mathrm{plotted}} = a\mathrm{FY}_{\mathrm{measured}} + b$, where a and b are constants independent of energy. The energies were $E_1 = 525$ eV and $E_2 = 550$ eV for Fig. 2(a) and $E_1 = 525$ eV and $E_2 = 560$ eV for Fig. 2(b).

The alignment normalizes out differences in the number of oxygen atoms. SL-A and SL-C FY scans in Fig. 2(a) differ at the MCP and SHP energies only. Because of the step size of energy scans, related to the monochromator energy resolution,

only a few data points sample the range of these two peaks. That the differences in FY at MCP and SHP are not random fluctuations is confirmed by measurements of the scattering contrast between the SL layers (Sec. II D).

SCO layers are prone to oxygen vacancies and LCO layers to oxygen interstitials. However, the difference in SHP intensity of SL-A and SL-C can not be due to these defects. Specifically, because MCP is higher in SL-A, this sample has a larger number of SCO layers compared to SL-C. Vacancies in these layers would reduce the intensity at SHP, as it happens in NCCOC [Fig. 2(a), inset], while hole doping, in contrast, would increase the SHP intensity. The SHP intensity is larger in SL-A. This points to hole doping in the SCO layers. Similarly, the difference in SHP intensity between SL-A and SL-C can not be due to interstitial atoms in LCO layers because SL-A has the larger SHP intensity, but relatively fewer LCO layers. Therefore, both differences between FY spectra (at MCP and SHP) are due to electronic contrast from doping, not to a structural defect, e.g., a vacancy or interstitial oxygen. These FY results are a clear indication that the ZRS-UHB model extension in our doping range beyond the MCP and UHB levels is related to doping SHP holes.

Within the experimental resolution, the SHP energy is relatively insensitive to the type of oxygen neighbors. For instance, it is not influenced by the Cu d states since Al^{3+} in LSAO has no d states or by replacing La with Sr. The FY increase from SL-C to SL-A is at the same energy (SHP) as the energy of a peak of the undoped LCO compound, which suggests that the SHP state, partly empty in undoped LCO, is gradually emptied further, rather then removed, with additional hole doping in SL-A compared to SL-C; that is, doping also makes holes at SHP. Therefore, the total numbers of doped MCP and SHP holes in one superperiod are related by the charge conservation equation as $\sum_l \langle t_l^{\mathrm{MCP}} \rangle + \sum_l \langle t_l^{\mathrm{SHP}} \rangle = 2N_{\mathrm{SCO}}$, where t is the occupation factor of site l, l sums over one superperiod, $\langle \ldots \rangle$ is the in-plane average, N_{SCO} is the number of SCO layers, and $2N_{\mathrm{SCO}}$ is the total number of doped holes in one superperiod (each $Sr_2CuO_{4-\delta}$ layer dopes 2 holes when $\delta \approx 0$).

Knowledge of the SCO oxygen vacancy site for $x = 2$ would suggest the site of the doped SHP hole; however, the question of the vacancy site is not settled.[18] The absence of this feature in the cuprate NCCOC, which does not have the apical oxygen (Fig. 2), suggests that SHP is an apical oxygen state. It is possible that SHP is absent in NCCOC for other reasons than the absence of the apical oxygen. For instance, in an alternative view of angle-resolved FY measurements on bulk LNO,[34,37] SHP are considered in-plane oxygen states mixed with Ni, and polarized in-plane. However, the SHP energy is not influenced by the Cu d states or replacing La with Sr, which suggests various hybridizations are not essential. The incipient out-of-plane doping for low x (Refs. 2 and 22) supports the view that doping is not confined to the CuO_2 planes for high x. Indeed, more detailed early calculations of the $La_{2-x}Sr_xCuO_4$ system[38] suggested that the shift with doping in the relative alignment of the in-plane [O(1)] oxygen and apical [O(2)] oxygen ionization potentials will eventually lead to the preferential emptying of the apical oxygen orbitals at larger x. If SHP is an apical state, the Cu ions would be surrounded by holes on all six neighboring oxygen atoms. This transition to a gradual emptying of apical oxygen orbitals, balancing the valences of all six oxygen atoms near a Cu site (this hole distribution is seen in undoped La_2NiO_4, Ref. 34) is a sensible intermediate step toward the process of vacancy creation in SCO. This kind of change with doping in the site of the doped holes has been seen in other cuprates, for instance, in $YBa_2Cu_3O_{6+\delta}$, where the holes stay mostly in chains in Cu and O orbitals up to $\delta \sim 0.25$, only then doping the oxygen states in the CuO_2 planes.[39,40]

To address the question of the orientation of the state behind SHP, angle-resolved FY measurements have been made [Fig. 2(b)]. A quantitative analysis of the angular dependence of FY requires measurements on bulk crystals cut at a series of angles with respect to the crystallographic planes to account for footprint and self-absorption effects.[36] Superlattice samples can not be grown at arbitrary angles. However, the SL footprint effects are almost identical for MCP and SHP energies because of the very similar scattering geometry. Self-absorption effects would have to be very strong for the observed suppression of intensity at SHP. That SL self-absorption effects are relatively small is supported by the very small difference in the momentum linewidth between MCP and SHP [Fig. 1(c), inset], which shows that the entire SL is probed at both energies. In addition, the O edge step height is approximately the same before the alignment in Fig. 2(b), which also suggests that self-absorption effects are relatively small at the O edge. We restrict our analysis of angle-resolved FY to a qualitative discussion.

The MCP and SHP intensities follow a similar angular dependence. We assume that the SHP state can be associated with a single orbital (if localized) or a collection of orbitals of the same type (if delocalized, as for the ZRS state, corresponding to MCP), in which case the SHP state would correspond to a band of a specific symmetry. The similar variation with angle of MCP and SHP intensity in angle-resolved FY measurements [Fig. 2(b)] suggests that the state corresponding to the SHP energy is oriented as the in-plane ZRS. Also, the MCP and SHP scattering amplitudes remain similar over a wide angular range (Fig. 4), which would be difficult to explain if they were polarized in different directions.

Therefore, our data provide evidence that SHP is a state at the apical oxygen site polarized in the a-b plane. The apical oxygen orbitals are $p_{x,y}$ pointing to Sr or La in the same LaO plane and orbitals of p_z symmetry from interactions with Cu and La ions in the neighboring CuO_2 and LaO planes. The only possibility consistent with this interpretation are the orbitals pointing to the La atoms in the same LaO plane.

C. Fluorescence yield and scattering at the La and Cu edges

RSXS can measure bulk[41–43] and SL (Refs. 35, 44, and 45) charge order. SL scattering measurements were made with π-polarized light at beamline X1B in an UHV diffractometer. Before the more complex SL reflectivity at the O edge, we present the measurements at the La and Cu edges, which will be used to illustrate the model of Sec. III A.

FY measurements at the La M_5 edge for SL-A and SL-C are shown in Fig. 3(a). The scattering contrast between the SL layers from $L = 1$ to 7, $\delta f_{\mathrm{SL}}^{(\mathrm{La})} = (f_{\mathrm{SCO}} - f_{\mathrm{LCO}})|_{\mathrm{La\,edge}}$, is given mainly by the difference between the number of

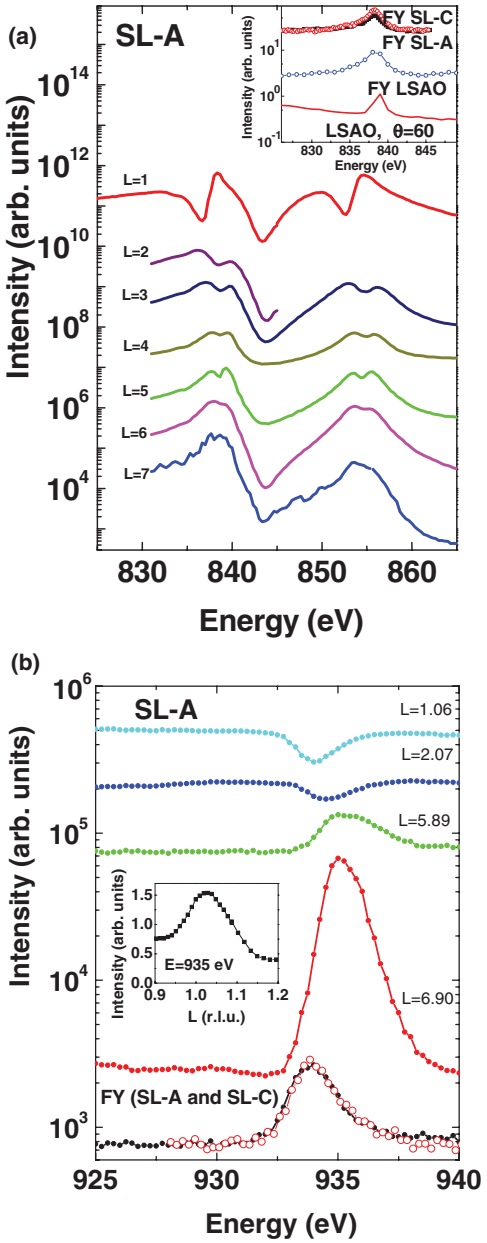

FIG. 3. (Color online) (a) Reflectivity at the La edge for SL-A. The plots have been shifted vertically for clarity. Inset: FY for SL-A and SL-C. The only clear difference in FY is an increase in the overall height, consistent with a larger number of La atoms in SL-C. The two lower curves are the LSAO substrate FY and reflectivity at $\theta = 60^\circ$, showing the strong resonant increase in the substrate reflectivity. The difference from measurements on SL is due to the absence of SL scattering contrast δf_{SL} (Sec. III A). (b) Line shapes at the Cu edge. For intermediate conditions, the scattering line shape is flat: this is observed for SL-C at $L = 4$ (not shown). The two-dimensional profile has a saddle point for $L = 1$: it is a peak when scanning L (inset) and a dip when scanning E. This is in contrast to multiple-scattering effects in HXD that can be observed for certain oxide SL, where a dip is present at integer L instead of a peak (data not shown). The lower curves compare the FY for SL-A (full symbols) and SL-C (open circles).

La atoms in the LCO and SCO layers $\langle t^{\mathrm{La}}_{l,\mathrm{LCO}}\rangle$ and $\langle t^{\mathrm{La}}_{l,\mathrm{SCO}}\rangle$. Consistent with this observation, there is a large nonresonant tail in scattering at the La edge for SL peaks, which was used to characterize the SL structure [Fig. 1(c)]. The line shape in Fig. 3(a) is approximately the same for different L because of the relatively small contribution from the surface reflectivity compared to the SL reflection (Sec. III A).

FY measurements at the Cu edge [Fig. 3(b)] are very similar for SL-A and SL-C; the scattering contrast at this edge is given by a small difference in the Cu valence, $\delta f^{(\mathrm{Cu})}_{\mathrm{SL}} = (f_{\mathrm{SCO}} - f_{\mathrm{LCO}})|_{\mathrm{Cu\,edge}}$, the difference in the dispersion corrections at the Cu edge between the SCO and LCO layers. Even for the SL higher doping levels, holes do not appear to empty unusual Cu states, unlike the case of $YBa_2Cu_3O_{6+\delta}$.[40] Small SL imperfections shift the peaks from integer values. The line shape changes with L from a dip on resonance (low L) to a peak (high L). This change is not due to absorption (the calculated absorption depth is much larger than the SL thickness), refraction (from two-dimensional profiles, data not shown), or multiple scattering at low L (similar effects are seen at high L in manganite SL, data not shown).

D. Scattering at the O edge

RSXS measurements at the O edge (Figs. 4 and 5) probe the spatial distribution of holes in the SL. Consistent with FY measurements (Sec. II B), the absence of a scattering peak at UHB shows that there is no contrast at this energy between SL layers. The scattering contrast in Fig. 4 occurs mostly at the two energies (MCP and SHP), where SL-A and SL-C differed in the FY (Fig. 2). Because this scattering peaks at SL reflections (Fig. 5), the charge density is modulated at MCP and SHP energies between SCO and LCO layers of the SL.

Sharpening of the features is observed at higher L (Fig. 4). The MCP and SHP peaks are well separated (the additional splitting of the MCP in SL-C will be discussed in Sec. III B). It is difficult to explain this clear separation with a difference in the energy of the same MCP hole state in the LCO and SCO layers, given the inherent interface roughness of the structure. This is strong evidence for considering SHP a qualitatively distinct hole state.

The low-L line shapes for SL-A, SL-B (not shown), and SL-C are more similar than the high-L line shapes because of the reduced importance of roughness (Sec. III B). At low L, the energy profiles show increased intensity between MCP and SHP [Figs. 4 and 5(a)], unlike the La M_5 and M_4 edges (Fig. 3). Although the O edge line shapes are more complex, they can be qualitatively analyzed with the same model as for the La and Cu edges (Sec. III A). The difference in the MCP and SHP line shapes at low L is due to different interference conditions with the surface reflection (Sec. III B).

Vacancies are present[18] in bulk SCO as well as at certain interfaces, even when the bulk materials do not contain vacancies.[48] If there were vacancies in the SCO layers or at interfaces, these would give a peak in scattering at all O edge energies. However, we do not observe large features above the SHP energy that would indicate a structural difference (either vacancies or oxygen atoms at interstitial sites) between the LCO and SCO layers (Fig. 5). Since the samples were annealed in ozone, the SCO layer thickness is relatively small, and there is little SL scattering at the O edge other than at

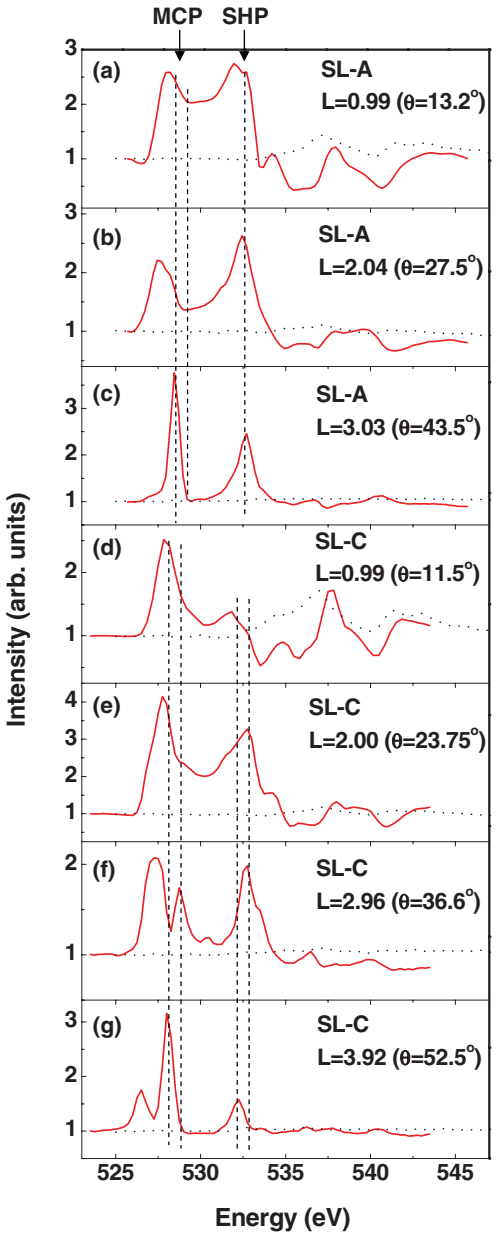

FIG. 4. (Color online) Line shapes at constant L for different SL peaks (solid line), compared to substrate reflectivity (dotted line) at the O edge, for SL-A [(a)–(c)] and SL-C [(d)–(g)]. Results on SL-B (not shown) were similar to those for SL-A, supporting the observation that small structural irregularities do not affect our conclusions. The scans have been normalized to unity below the edge. SL-A and SL-C have different scattering line shapes at high L because of different SL roughness and structure (Sec. III B). Measurements on the substrate, approximating the surface reflectivity S_0 (Sec. III A), show that the surface reflectivity resonant contribution gets negligible at higher L, where the substrate reflectivity becomes more featureless. Vertical dashed lines are guides to the eye.

MCP and SHP (Fig. 5), we will neglect vacancies in the following analysis, that is $\delta \approx 0$. The number of oxygen atoms is approximately the same throughout the SL, while their valence is different in the SCO and LCO layers, giving the scattering contrast. Therefore, SL scattering at the MCP and SHP energies probes the difference between SCO and LCO

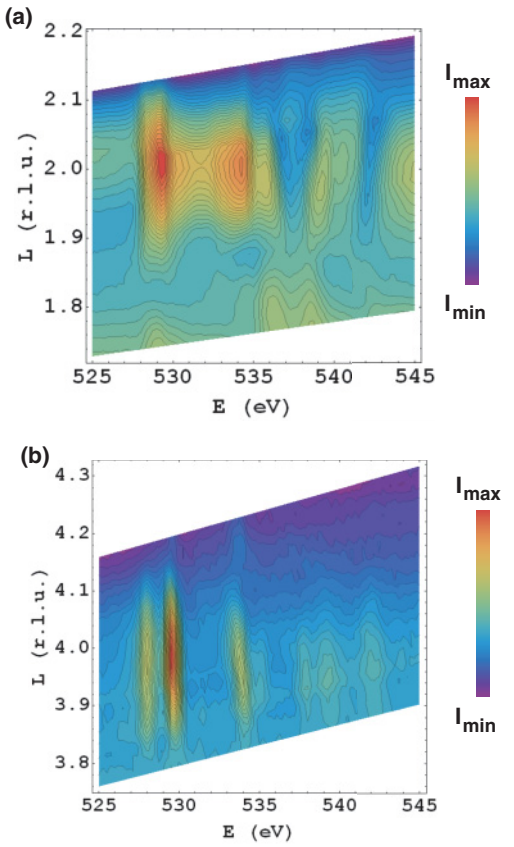

FIG. 5. (Color online) Two-dimensional plots in variable energy E and momentum L for two selected SL peaks. For the relative intensities, cuts through these plots are shown in Figs. 4(e) and 4(g). (a) Scattering two-dimensional resonance profile (logarithmic color scale) for SL-C near $L = 2$ at the O edge shows the mirror symmetry of the MCP and SHP scattering line shapes. Same results were obtained for SL-A and SL-B. (b) Scattering two-dimensional resonance profile (logarithmic color scale) for SL-C near $L = 4$ at the O edge shows that the MCP and SHP holes are qualitatively different.

layers form factors $\delta f_{\rm SL}^{\rm (MCP,SHP)} = (f_{\rm SCO} - f_{\rm LCO})|_{\omega={\rm MCP,SHP}}$, measuring the change in the dispersion corrections with doping.

III. DISCUSSION

The x-ray scattering intensity is $I = A|S|^2$, with the structure factor given by

$$S(\omega, Q) = \sum_{l,n} f_n(\omega, Q) t_l^n e^{iQz_l}, \qquad (1)$$

where ω is the incident x-ray energy, $Q = (0,0,2\pi L/c_{\rm SL})$ is the scattering momentum in the reflectivity geometry, and t_l^n is the occupation factor in atomic plane l of element and valence n.[45] The form factor $f(\omega, Q)$ for soft x-ray momenta is $f(\omega, Q) = f^0(Q) + f'(\omega) + if''(\omega) \approx f^0(0) + f'(\omega) + if''(\omega)$. For only one source of scatterers ($n = 1$) and scalar form factor f, the variables ω and Q in the structure factor $S(\omega, Q)$ are separable, that is, $S(\omega, Q) = f(\omega)h(Q)$.

Since f is in general a tensor, we explain why the above considerations are valid in the case of resonances at the O

K and Cu L edges. In general, for tensors f^{ij} with only one independent functional dependence on energy ω [$f(\omega)$], dotting the indices i and j of the f^{ij} matrix with the initial and final light polarization vectors necessarily results in an expression $f(\omega)T(\theta)$, which is proportional to $f(\omega)$. The difference from the scalar case is only in the term multiplying $f(\omega)$ [$T(\theta)$ or $T(L)$], which, because it does not depend on energy, can be included in the arbitrary units. Then, for this special tensor case, the structure factor is separable, as it is for scalar f.

Specifically, for the contrast between the SL layers $\delta f_{\rm SL}$, the indices i and j are dotted with the light polarization vectors $\hat{\epsilon}_{\rm final}$ and $\hat{\epsilon}_{\rm initial}$ as $\delta f_{\rm SL} = \hat{\epsilon}^*_{i,\rm final}\delta f^{ij}_{\rm SL}\hat{\epsilon}_{j,\rm initial}$. Momentum-dependent measurements, for instance, of the small ridge in scattering before the edge at the O K edge (Fig. 5), show that the nonresonant contribution is small in $\delta f_{\rm SL} = f_{\rm SCO} - f_{\rm LCO}$. Then, only one independent component of $\delta f^{ij}_{\rm SL}$, namely, the in-plane $\delta f^{xx}_{\rm SL} = \delta f^{yy}_{\rm SL}$, remains for resonances at the Cu edge, at MCP, as well as at SHP from the similar angular dependence of FY (Sec. II B). In this case, the angular dependence given by the double product simplifies to $S \propto \hat{\epsilon}^*_{i,\rm final}\delta f^{ij}_{\rm SL}\hat{\epsilon}_{j,\rm initial} \propto \delta f^{xx}_{\rm SL}(\omega)\sin^2(\theta)$, with an additional factor [$\sin^2(\theta)$] that can be absorbed into the arbitrary units. This implies identical line shapes (up to an overall scaling factor) for the same edge at all L. This is not observed at the Cu edge or for the MCP state [Figs. 3(b) and 4]. Therefore, at least two scattering sources ($n > 1$), interfering in the total structure factor $S(\omega, L)$, need to be considered. "Stray light" only contributes an overall background level. To interfere, the contributions to $S(\omega, L)$ must be coherent and of the same energy.

One possibility is to include additional terms to $S(\omega, L)$ modeling structural distortions. When these terms are considered, the ω and L variables are no longer separable in $S(\omega, L)$. A difference in the line shapes at different reflections has been observed with hard x rays at transition-metal K edges,[46] related to contributions to the structure factor from such terms. However, structural distortion terms increase with increasing momentum and can not explain our measurements at the Cu edge, where the nonresonant intensity is relatively small at high L and the line shape is strongly modified at low L (Fig. 3). The different angular dependence of resonant and nonresonant scattering intensity from different polarizations does not account for the observed small nonresonant intensity at high L at the Cu edge and, based on this, we neglect nonresonant terms of this type. Another nonresonant term, which is large at low L and can explain our observations, is the surface reflection.

A. Scattering model

To analyze the line shapes at the O edge shown in Fig. 4, we develop a model for the interference between the surface and a SL reflection. With the above approximation for $f(\omega, Q)$, the structure factor for more than one type of scatterer (the condition of a SL) becomes

$$S^{ij}(\omega, L) = \sum_n f^{ij}_n(\omega) \sum_l \langle t^n_l \rangle e^{2\pi i L z_l / c_{\rm SL}}, \qquad (2)$$

where $\rho^n(L) = \sum_l \langle t^n_l \rangle e^{2\pi i L z_l / c_{\rm SL}}$ is the Fourier transform of the distribution $\{\langle t^n_l \rangle\}$ of in-plane averages of the occupation factors for layer l and element and valence n. Considering only two elements, $n =$ A and B as an example, arranged in a semi-infinite SL structure extending into half-space (bounded by a surface), and $\langle t^{\rm A}_l \rangle + \langle t^{\rm B}_l \rangle = 1$ for all l, we obtain a total structure factor $S^{ij}(\omega, L) = S^{ij}_0 + S^{ij}_{\rm SL}$ made of two terms:

$$S^{ij}_0 = \left(f^{ij}_{\rm A} \frac{N_{\rm A}}{N} + f^{ij}_{\rm B} \frac{N_{\rm B}}{N} \right) \rho_{0,\rm SL} = f^{ij}_{0,\rm SL} \rho_{0,\rm SL} \qquad (3)$$

and

$$S^{ij}_{\rm SL} = \left(f^{ij}_{\rm B} - f^{ij}_{\rm A} \right) \left[\rho^{(\rm B)}_{\rm SL} \frac{N_{\rm A}}{N} - \rho^{(\rm A)}_{\rm SL} \frac{N_{\rm B}}{N} \right] = \delta f^{ij}_{\rm SL} \rho_{\rm SL}, \qquad (4)$$

where $N_{\rm A}$, $N_{\rm B}$, $N = N_{\rm A} + N_{\rm B}$ are the number of ML in one A layer, one B layer and one superperiod, $f^{ij}_{0,\rm SL}$ is the average of the SL layers form factors, $\delta f^{ij}_{\rm SL} = f^{ij}_{\rm B} - f^{ij}_{\rm A}$ is the contrast between the form factors of the SL layers. The $S_{\rm SL}$ term describes SL reflections, broadened along L in Fig. 6(b), according to the spatial distribution of the atoms in the SL. The S_0 term describes the (000), (002), etc., reflections of the LSCO unit cell, broadened into the crystal truncation rods in Fig. 6(b) along scattering momenta L, normal to the surface.

A complex oxide SL has more than two constitutive elements. We neglect for soft x-ray momenta the small difference in z_l between the SrO/LaO and CuO_2 planes within 1 ML, or equivalently between oxygen sites O(1) (in plane) and O(2) (apical). In this case, f_0 becomes the average total form factor and Eqs. (3) and (4) can be applied by replacing $\rho^{(\rm A,B)}_{\rm SL}$ with $\rho^{(\rm LCO,SCO)}_{\rm SL}$, $N_{\rm A,B}$ with $N_{\rm LCO,SCO}$, and $f_{\rm A,B}$ with $f_{\rm LCO,SCO}$, the total form factors of 1 ML. The $S_{\rm SL}$ term is the reflection from the SL modulation. The modulation of the density of La and Sr atoms in the SL also gives modulations of the form factors at the Cu ($\delta f^{(\rm Cu)}_{\rm SL}$) and O ($\delta f^{(\rm MCP,SHP)}_{\rm SL}$) edges.

The S_0 term in Eq. (3) gives the reflection from the discontinuity in the index of refraction n, or equivalently in the average form factor $f_{0,\rm SL}$, at the sample surface. For a SCO/LCO SL, $f_{0,\rm SL} = \frac{N_{\rm LCO}}{N}(2f_{\rm La}) + \frac{N_{\rm SCO}}{N}(2f_{\rm Sr}) + f_{\rm Cu} + 4f_{\rm O}$, which can be calculated from tabulated[49] values. $f_{0,\rm SL}$ is made mostly of nonresonant terms at the Cu and O edges (but not at the La edge[47]) and, because of this, does not depend strongly on energy or polarization. Considering the substrate extends the sum in Eq. (2) to an infinite number of layers, with the function $\rho_{0,\rm SL}$ replaced by $\rho_0(L) = 1/(1 - e^{2\pi i L/N})$ and $f_{0,\rm SL}$ replaced by $f_0 = (1 - \tau) f_{0,\rm SL} + \tau f_{0,\rm LSAO}$, where $f_{0,\rm LSAO}$ is the substrate contribution and $\tau(\theta, 2\theta, \omega)$ is a weighting factor which depends on the scattering geometry $(\theta, 2\theta)$ and energy (ω) through a variable absorption depth. Therefore, the interference at different edges will be analyzed in terms of two main components: a SL reflection $S_{\rm SL}$ and a surface reflection S_0 [Fig. 6(a)].

The momentum dependence of S_0 and $S_{\rm SL}$ in Eqs. (3) and (4) is contained in the functions $\rho_{0,\rm SL}$, $\rho^{(\rm LCO)}_{\rm SL}$, and $\rho^{(\rm SCO)}_{\rm SL}$. For a SCO/LCO superlattice with no roughness, they are (r is the number of repeats)

$$\rho_{0,\rm SL} = \sum_{l,\,All} e^{2\pi i L z_l / c_{\rm SL}} = \frac{1 - e^{2\pi i L r}}{1 - e^{2\pi i L/N}}, \qquad (5)$$

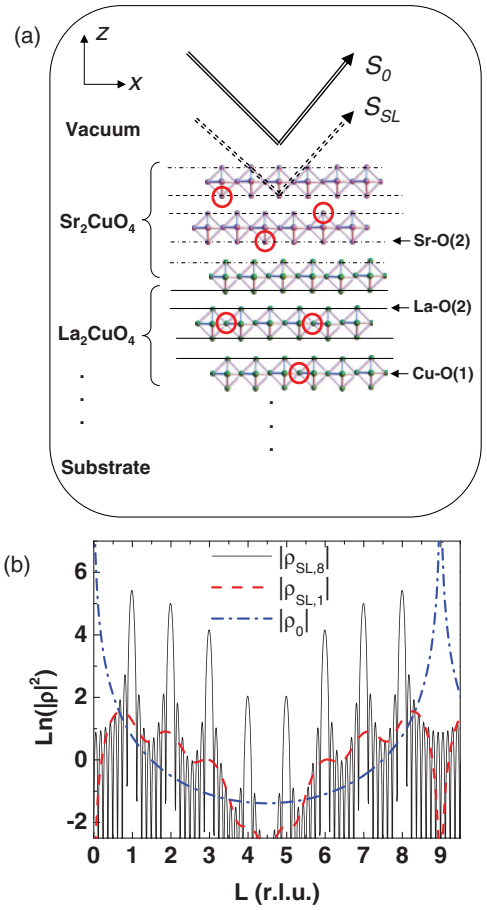

FIG. 6. (Color online) (a) Sketch of the two components in the structure factor S: the surface S_0, from the discontinuity between the vacuum and the surface, and S_{SL}, from the modulation δf_{SL} between SCO and LCO layers. The circles show the location of the MCP and SHP holes doped in the LCO and SCO layers, if the SHP is scattering from a hole on an orbital at the apical O(2) sites (Sec. II B). A few examples of atomic planes in the SCO and LCO layers are indicated. (b) Calculations of $|\rho_{SL,8}(L)|$ and $|\rho_{SL,1}(L)|$ for a [2 × SCO + 7 × LCO] SL with no roughness and 8 and 1 repeats, compared to the surface $|\rho_0(L)|$. The (000) and (009) reflections in units of the SL superperiod c_{SL} are the (000) and (002) reflections of the LSCO unit cell spread into crystal truncation rods.

$$\rho_{SL}^{(LCO)} = \sum_{l,LCO} e^{2\pi i L z_l / c_{SL}}, \tag{6}$$

and

$$\rho_{SL}^{(SCO)} = \sum_{l,SCO} e^{2\pi i L z_l / c_{SL}} = \rho_{0,SL} - \rho_{SL}^{(LCO)}. \tag{7}$$

Except near $L = mN$, where m is an integer, the functions $\rho_{SL}^{(LCO)}$ and $\rho_{SL}^{(SCO)}$ are related as $\rho_{SL}^{(LCO)} \approx -\rho_{SL}^{(SCO)}$. Therefore, they are out-of-phase:

$$\mathrm{Arg}\left[\rho_{SL}^{(LCO)}(L)\right] = \pi + \mathrm{Arg}\left[\rho_{SL}^{(SCO)}(L)\right], \tag{8}$$

where $\mathrm{Arg}[\rho_{SL}^{(LCO)}(L)] = \pi L(N_{LCO} - 1)/N$.

Figure 6(b) shows the functions $|\rho_0(L)|$ and $|\rho_{SL}(L)|$ for a 8 × [2 × SCO + 7 × LCO] structure. The L dependence of $|\rho_0|$ and $|\rho_{SL}|$ is very different; while $|\rho_0|$ has peaks at $L = mN$, where m is an integer, $|\rho_{SL}|$ follows a momentum dependence with pronounced peaks at integer $L \neq mN$. $|\rho_{SL}|$ is therefore much higher than $|\rho_0|$ at these L values: $|\rho_{SL}| \gg |\rho_0|$. It would appear that the surface reflection can be neglected near SL reflections. However, $|f_0|$ is considerably larger than $|\delta f_{SL}(\omega)|$ at certain edges, with the SL and surface structure factors comparable in magnitude $|S_{SL}| \sim |S_0|$.

Including both terms, the intensity of x-ray scattering can be written as

$$I = A|\rho_{SL}|^2 \left|\delta f_{SL} + \frac{f_0 \rho_0}{\rho_{SL}}\right|^2 = A' \left|\delta f_{SL}(\omega) + z_L\right|^2 \tag{9}$$

with $|\rho_{SL}|^2$ (independent of ω) absorbed into the arbitrary units. It is not possible at present to calculate from first principles the energy-dependent form factor $\delta f_{SL}(\omega)$ for a correlated oxide SL. However, FY measurements (Fig. 2) show that the energies of MCP and SHP do not depend on the environment of the oxygen atom, which suggests a simplified model. Therefore, the line shapes at different edges will be modeled with a harmonic-oscillator functional dependence. The function used for the imaginary part of the form factor is $\delta f''_{SL}(\omega) = \frac{\alpha E}{(E-E_0)^2+\Gamma^2}$. This is Kramers-Kronig transformed to obtain the real part $\delta f'_{SL}(\omega)$ [Fig. 7(a)]. Figure 7(b) shows $|\delta f_{SL} + z_L|$ for different z_L.

The interference between the surface S_0 and superlattice S_{SL} terms can qualitatively describe the scattering line shapes at all edges. At the La edge, $|\delta f_{SL}^{(La)}|$ is comparable to $|f_0|$, $|S_{SL}| \gg |S_0|$ and little change of the resonance line shapes with L is expected. Indeed, there is little change with L at the La edge [Fig. 3(a)], except at low L. Measurements on the substrate at the La edge [Fig. 3(a), inset] indicate a strong resonance in f_0, which is responsible for the variation in the line shape at low L. Specifically, refraction effects shift the peaks and complicate the interpretation of the measurements at low L; because of this, the measurements at the La edge will be discussed in detail separately.[47] The scattering line shape at the M_5 and M_4 edges has the same shape because it originates in states on the same La atoms; this is in contrast to the scattering at the O edge at low L, where the line shape at the MCP and SHP resonances is different (Sec. III B).

At the Cu edge, $\delta f_{SL}^{(Cu)}$ is the change in the dispersion corrections with doping and, because of the small modulation in the Cu valence, $|\delta f_{SL}^{(Cu)}| \ll |f_0|$ and $|S_{SL}| \ll |S_0|$. Strong interference effects are expected and observed [Fig. 3(b)]. The scattering shows a strong surface contribution to reflectivity. The nonresonant ($f_{0,SL}$ and $f_{0,LSAO}$) form factors have large imaginary parts f_0'' because of the neighboring La edge and the line shapes resemble those of panels (2) and (8) in Fig. 7(b). The O edge scattering, with $|S_{SL}| \sim |S_0|$, is an intermediate case. $\delta f_{SL}^{(MCP,SHP)}$ is relatively large and f_0'' is smaller than at the Cu edge, with the line shapes in a different region of Fig. 7(b): for low L, the MCP and SHP are of the type (4) and (6), and for high L of the type (5) and (2). Scattering line shapes are the most variable, with large complex changes with L. The scattering at the O edge is analyzed in more detail in the next section.

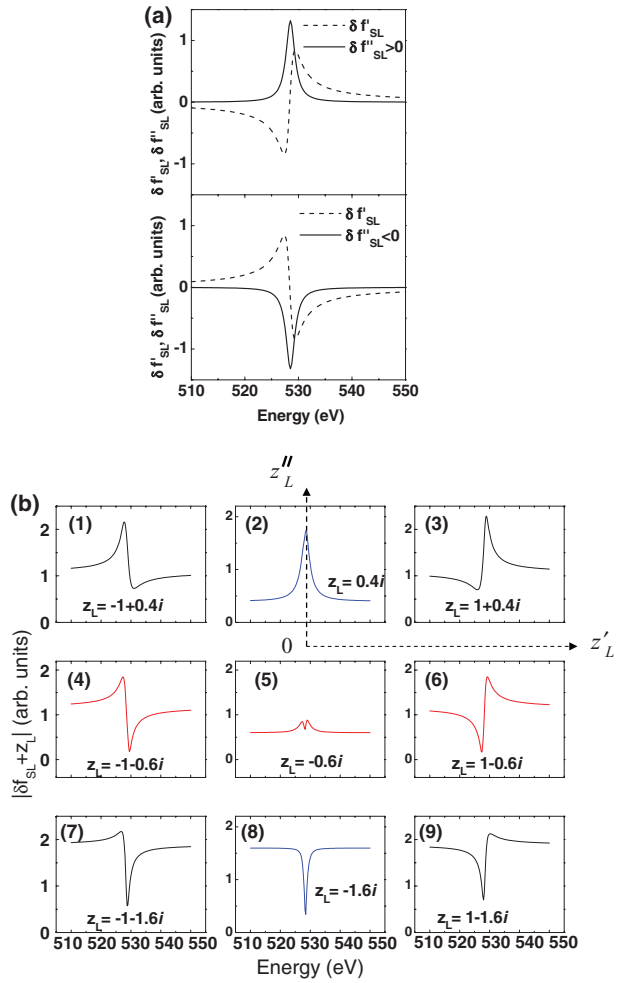

FIG. 7. (Color online) (a) $\delta f''_{\rm SL} = f''_{\rm SCO} - f''_{\rm LCO}$ is the difference of two f'' and can have in principle either sign. Functions $\delta f''_{\rm SL}$ and $\delta f'_{\rm SL}$ obtained by Kramers-Kronig transform. The parameters were $\alpha = 2.5 \times 10^{-3}$ (top) and $\alpha = -2.5 \times 10^{-3}$ (bottom), $E_0 = 528.5$ eV and $\Gamma = 1$ eV. The sign convention with $f'' = +\sigma_{\rm abs}/(2r_0\lambda)$ has been used. (b) Line shapes $|\delta f_{\rm SL} + z_L|$ calculated for different interference conditions, arranged in the (z'_L, z''_L) plane according to the z_L term used, show the variety of behaviors at the Cu edge [panels (2) and (8)], La edge [panel (4)], and O edge [panels (4) and (6)].

B. Locus of MCP and SHP scatterers

Interference between the surface and the SL reflections determines the line shape. This can be used to find the locus of the MCP and SHP scatterers within the SL structure. In this section, it is first shown that $\delta f_{\rm SL}^{\rm (MCP)}$ and $\delta f_{\rm SL}^{\rm (SHP)}$ scattering is similar in shape. Then, with the neglect for low L of the small z_l differences between atoms within 1 ML (Sec. III A), the relative phase between these two scatterers left to explain the observed different line shapes is the relative phase given by the spatial separation between the LCO and SCO layers.

As pointed out, the functions $\delta f_{\rm SL}^{\rm (MCP,SHP)}$ can not be calculated. However, the change with doping in the dispersion corrections at MCP and SHP energies can be estimated by looking at the difference in FY ($\delta f''_{\rm FY} = f''_{\rm SL\text{-}A} - f''_{\rm SL\text{-}C}$) between *two* differently doped SL, which gives the scattering contrast between SL *layers* ($\delta f''_{\rm SL} = f''_{\rm SCO} - f''_{\rm LCO}$) in *one* SL (either SL-A or SL-C). Specifically, when comparing SL-A with SL-C, FY intensity increases concurrently at MCP and SHP [Fig. 2(a)]. Therefore, for both MCP and SHP energies, the difference in the dispersion corrections $\delta f''_{\rm SL}$ in the SCO and LCO layers is positive:

$$\delta f''_{\rm SL}({\rm MCP,SHP}) \propto \delta f''_{\rm FY}({\rm MCP,SHP}) > 0. \qquad (10)$$

The Kramers-Kronig transform of a $\delta f''_{\rm SL} > 0$ peak gives the shape shown in Fig. 7(a) (top panel) for $|\delta f_{\rm SL}| = |\delta f'_{\rm SL} + i\delta f''_{\rm SL}|$.

However, measurements show line shapes for the MCP and SHP states with a mirror symmetry at $L = 1$ and 2 (Figs. 4 and 5). It is necessary therefore to consider the contribution to scattering of z_L, the other factor in Eq. (9). Measured line shapes for MCP [of type (3)-(6)-(9), right side] and SHP [of type (1)-(4)-(7), left side] are on opposite sides of the complex (z'_L, z''_L) plane in Fig. 7(b). Therefore, $z_L^{\rm (MCP,SHP)}$ for MCP and SHP have opposite phases.

Considering the factors combined in $z_L^{\rm (MCP,SHP)}$, since ρ_0 is the same at MCP and SHP and f_0 can not change sign over the ~ 4 eV between the MCP to SHP energies, as evidenced by the weak energy dependence of the substrate reflection (Fig. 4) and the large nonresonant component of f_0, the difference between $z_L^{\rm (MCP,SHP)}$ must be in $\rho_{\rm SL}^{\rm (MCP,SHP)}(L)$, the Fourier transforms of the distributions $\{\langle t_l^{\rm (MCP)}\rangle\}$ and $\{\langle t_l^{\rm (SHP)}\rangle\}$ of the occupation factors at the two energies. Because z_L and $\rho_{\rm SL}$ are inversely proportional, $\rho_{\rm SL}$ also has opposite phases at the MCP and SHP energies:

$${\rm Arg}\left[\rho_{\rm SL}^{\rm (MCP)}(L)\right] = \pi + {\rm Arg}\left[\rho_{\rm SL}^{\rm (SHP)}(L)\right]. \qquad (11)$$

Therefore, the distributions $\rho_{\rm SL}^{\rm (MCP,SHP)}(L)$ are out-of-phase, with the spatial distributions of the MCP and SHP holes [Eq. (11)] related in the same way as the spatial distributions of the LCO and SCO layers in the SL [Eq. (8)]. Then, it is necessary that the MCP and SHP hole distributions peak in different layers.

This conclusion, using measurements at low L, where roughness effects are less important, is independent of the thickness of LCO and SCO layers in one superperiod or roughness amplitude. Roughness effects become more important at higher L, where the MCP and SHP line shapes resemble line shapes closer to the origin of the complex plane in Fig. 7(b). To qualitatively explain the difference between line shapes at high L for SL-A and SL-C, we consider the L dependence of the intensity in Eq. (9), contained in the z_L phase and amplitude. The z_L phases for the MCP and SHP holes follow those of the LCO and SCO layers, which are linear functions of L: ${\rm Arg}[z_L^{\rm (LCO)}] = {\rm Arg}[f_0] + \pi L N_{\rm SCO}/N$ and ${\rm Arg}[z_L^{\rm (SCO)}] = {\rm Arg}[z_L^{\rm LCO}] + \pi$. The other contributing factor to the change in the line shape with L is the variation in the z_L amplitude. For Gaussian roughness, the ratio $|\rho_0/\rho_{\rm SL}|$ in $|z_L|$ depends on the surface σ_s and the interface σ_i roughness as $|\rho_0/\rho_{\rm SL}| = |\rho_0/\rho_{\rm SL}|_{\rm ideal} R(Q_z)$, where $R(Q_z) = e^{-(\sigma_s^2 - \sigma_i^2)Q_z^2/2}$ and $Q_z = 2\pi L/c_{\rm SL}$. The factor $R(Q_z)$ becomes increasingly important at higher L. Therefore, the linear increase of the z_L phase with L and the reduction in the amplitude of $|z_L| = |z_L|_{\rm ideal} R(Q_z)$ at higher L for $\sigma_s > \sigma_i$ combine to make the vector z_L spiral inward in the (z'_L, z''_L) plane of Fig. 7(b) with increasing L, systematically sampling different line shapes at the same edge.

Figure 4(c) for SL-A, with the first peak in the split MCP almost absent, shows the interference line shape in a slightly different location in the plane of Fig. 7(b) than the location corresponding to the line shape in Fig. 4(g) for SL-C, where both peaks are visible at MCP. This divergence between measurements for SL-A and SL-C with increasing L (Fig. 4) can now be explained by considering the different roughness of SL-A and SL-C. SL-A has a larger surface σ_s than SL-C (Sec. II A), but similar interface roughness σ_i. Therefore, $R(Q)$ is smaller for SL-A, which makes the end of the z_L vectors for SL-A and SL-C follow slightly different trajectories with increasing L in the plane of Fig. 7(b). A quantitative discussion of roughness effects is postponed.

The interference between S_{SL} and S_0, resembling multiwavelength anomalous diffraction in molecular crystallography, allows determining the superlattice MCP and SHP hole distributions on a relatively large scale. To confirm the FY measurements of Sec. II B and the site of the SHP state within 1 ML, a fit with the interference model of Sec. III A would be necessary for higher wave vectors ($L > 2$), giving better spatial resolution. In future work, fitting the evolution of measured interference line shapes (Figs. 4 and 5) with L would also allow obtaining $\delta f_{\mathrm{SL}}^{(\mathrm{MCP,SHP})}$, σ_s and the energy-dependent σ_i (on which the z_L amplitude depends), and N_{SCO} or N_{LCO} (on which the z_L phase depends).

The MCP and SHP hole distributions, maximized in different layers, are consistent with the saturation of FY in Ref. 25 and observations in Ref. 38, where the apical hole site is favored at high doping. The relatively smaller number of MCP holes in the SCO layers is consistent with the observation that the MCP holes are mobile.[35] In contrast, remotely doping a new distinct type of holes at SHP in the LCO layers from the Sr in the SCO layers is an unlikely strong long-range process and the SHP holes remain centered on the SCO layers. The distributions of MCP and SHP holes are illustrated in Fig. 6(a).

IV. CONCLUSION

Measurements of doped LSCO at $x \lesssim 0.2$, for the same parent compound (LCO) with the same dopant (Sr) as our case, observed changes at MCP and UHB (Ref. 2). Using x-ray absorption and resonant soft x-ray scattering, we found that doping in SCO/LCO superlattices at high x empties two distinct oxygen states at MCP and SHP. X-ray absorption measurements suggest that the hole state at the higher energy is on apical oxygen atoms and polarized in the a-b plane. Since the creation of a vacancy removes two holes, this would suggest that the vacancies in bulk SCO are at the apical sites as well. A more complete doping sequence emerges for the LSCO material system. Holes are made on in-plane oxygen atoms[2] at low x. p_z holes are added to apical oxygen atoms at larger x (Refs. 21 and 22). For the doping range of this work, apical holes on $p_{x,y}$ orbitals are present. Finally, doped holes are partially removed with the creation of vacancies near $x = 2$.

The location of subsurface scatterers within the superlattice was determined using the interference with the surface reflection, with the distributions of the two hole states maximized in different layers. The interference between S_{SL} and S_0 may be compared to the interference in multiwavelength anomalous diffraction (MAD), which similarly utilizes dispersion corrections of resonant scattering and relative phases to determine a structure.[50] However, the nonresonant terms are different in the two cases. For MAD, scattering from the structure to be determined contributes to the nonresonant term. These nonresonant contributions are small for $\delta f_{\mathrm{SL}} = f_{\mathrm{SCO}} - f_{\mathrm{LCO}}$, the scattering contrast between the SL layers. Instead, the nonresonant term is given in our case by the intensity of the surface reflection S_0, broadened into crystal truncation rods. X-ray interference between overlayer scattering and nonresonant crystal truncation rods has been used before for structure determination with an analysis of nonresonant momentum scans.[51] In contrast, energy scans are analyzed in the interference model presented here.

The increase in the density of the unoccupied states at SHP has to come from an occupied state. Photoemission experiments to determine if a change with doping occurs in the density of states of occupied states that mirrors the change with doping seen at SHP in this study would be interesting. Calculations showed that making in-plane axial orbitals more localized, by gradually spatially removing the apical oxygen atoms, increases T_c,[7] and that, conversely, unoccupied apical oxygen p_z orbitals lower T_c. If similar ideas are applied to the SHP state, the doping of SHP holes might be responsible for the decrease of T_c and the hole pair breaking at $x > x_{\mathrm{optimal}}$,[52] and their partial removal, with the appearance of vacancies in SCO near $x = 2$, for the high T_c of bulk SCO.

ACKNOWLEDGMENTS

We thank A. Gozar for useful discussions. This work was supported by the Center for Emergent Superconductivity, an Energy Frontier Research Center funded by the US Department of Energy, Office of Science, Office of Basic Energy Sciences. Use of the NSLS was supported by DOE Grant No. DE-AC02-98CH10886. A.R. was supported by MOE AcRF Tier-2 Grant No. (MOE2010-T2-2-121) and NRF CRP.

*Present address: Max-Planck-Institut for Solid State Research, Heisenberg Strasse 1, D-70569, Stuttgart, Germany.

[1] H. Eskes and G. A. Sawatzky, Phys. Rev. B **44**, 9656 (1991).

[2] C. T. Chen, F. Sette, Y. Ma, M. S. Hybertsen, E. B. Stechel, W. M. C. Foulkes, M. Schluter, S.-W. Cheong, A. S. Cooper, L. W. Rupp, Jr., B. Batlogg, Y. L. Soo, Z. H. Ming, A. Krol, and Y. H. Kao, Phys. Rev. Lett. **66**, 104 (1991).

[3] K. Tanaka, T. Yoshida, A. Fujimori, D. H. Lu, Z.-X. Shen, X.-J. Zhou, H. Eisaki, Z. Hussain, S. Uchida, Y. Aiura, K. Ono, T. Sugaya, T. Mizuno, and I. Terasaki, Phys. Rev. B **70**, 092503 (2004).

[4] F. Ronning, C. Kim, D. L. Feng, D. S. Marshall, A. G. Loeser, L. L. Miller, J. N. Eckstein, I. Bozovic, and Z.-X. Shen, Science **282**, 2067 (1998).

[5]C. Di Castro, L. F. Feiner, and M. Grilli, Phys. Rev. Lett. **66**, 3209 (1991).
[6]L. F. Feiner, M. Grilli, and C. Di Castro, Phys. Rev. B **45**, 10647 (1992).
[7]E. Pavarini, I. Dasgupta, T. Saha-Dasgupta, O. Jepsen, and O. K. Andersen, Phys. Rev. Lett. **87**, 047003 (2001).
[8]D. M. deLeeuw, W. A. Groen, L. F. Feiner, and E. E. Havinga, Phys. C (Amsterdam) **166**, 133 (1990).
[9]Y. Ohta, T. Tohyama, and S. Maekawa, Phys. Rev. B **43**, 2968 (1991).
[10]W. G. Yin and W. Ku, Phys. Rev. B **79**, 214512 (2009).
[11]R. Raimondi, J. H. Jefferson, and L. F. Feiner, Phys. Rev. B **53**, 8774 (1996).
[12]H. Yang, Q. Q. Liu, F. Y. Li, C. Q. Jin, and R. C. Yu, Appl. Phys. Lett. **88**, 082502 (2006).
[13]M. Al-Mamouri, P. P. Edwards, C. Greaves, and M. Slaski, Nature (London) **369**, 382 (1994).
[14]J. H. Choy, W. Lee, and S.-J. Hwang, Phys. C (Amsterdam) **322**, 93 (1999).
[15]Y. Shimakawa, J. D. Jorgensen, J. F. Mitchell, B. A. Hunter, H. Shaked, D. G. Hinks, R. L. Hitterman, Z. Hiroi, and M. Takano, Phys. C (Amsterdam) **228**, 73 (1994).
[16]H. Zhang, Y. Y. Wang, L. D. Marks, V. P. Dravid, P. D. Han, and D. A. Payne, Phys. C (Amsterdam) **255**, 257 (1995).
[17]H. Yang, Q. Q. Liu, F. Y. Li, C. Q. Jin, and R. C. Yu, Phys. C (Amsterdam) **467**, 59 (2007).
[18]T. H. Geballe and M. Marezio, Phys. C (Amsterdam) **469**, 680 (2009).
[19]D. C. Johnston, Phys. Rev. Lett. **62**, 957 (1989).
[20]S. Wakimoto, R. J. Birgeneau, A. Kagedan, H. Kim, I. Swainson, K. Yamada, and H. Zhang, Phys. Rev. B **72**, 064521 (2005).
[21]C. T. Chen, L. H. Tjeng, J. Kwo, H. L. Kao, P. Rudolf, F. Sette, and R. M. Fleming, Phys. Rev. Lett. **68**, 2543 (1992).
[22]E. S. Bozin and S. J. L. Billinge, Phys. Rev. B **72**, 174427 (2005).
[23]V. Y. Butko, G. Logvenov, N. Bozovic, Z. Radovic, and I. Bozovic, Adv. Mater. **21**, 3644 (2009).
[24]S. Karimoto, H. Yamamoto, H. Sato, A. Tsukada, and M. Naito, J. Low Temp. Phys. **131**, 619 (2003).
[25]D. C. Peets, D. G. Hawthorn, K. M. Shen, Y.-J. Kim, D. S. Ellis, H. Zhang, S. Komiya, Y. Ando, G. A. Sawatzky, R. Liang, D. A. Bonn, and W. N. Hardy, Phys. Rev. Lett. **103**, 087402 (2009).
[26]X. Wang, L. de Medici, and A. J. Millis, Phys. Rev. B **81**, 094522 (2010).
[27]Y. Shimakawa, J. D. Jorgensen, J. F. Mitchell, B. A. Hunter, H. Shaked, D. G. Hinks, and R. L. Hitterman, Phys. C (Amsterdam) **228**, 73 (1994).
[28]P. G. Radaelli, D. G. Hinks, A. W. Mitchell, B. A. Hunter, J. L. Wagner, B. Dabrowski, K. G. Vandervoort, H. K. Viswanathan, and J. D. Jorgensen, Phys. Rev. B **49**, 4163 (1994).
[29]I. Bozovic, IEEE Trans. Appl. Supercond. **11**, 2686 (2001).
[30]I. Bozovic, A. Gozar, G. Logvenov, A. Bollinger, N. Bozovic, and Z. Radovic, J. Supercond.: Novel Magnetism **22**, 223 (2009).
[31]S. Hendricks and E. Teller, J. Chem. Phys. **10**, 147 (1942).
[32]S. Hulbert, D. J. Holly, F. H. Middleton, and D. J. Wallace, Nucl. Instrum. Methods Phys. Res., Sect. A **291**, 343 (1990).
[33]F. de Groot, Coord. Chem. Rev. **209**, 31 (2005).
[34]P. Kuiper, J. van Elp, G. A. Sawatzky, A. Fujimori, S. Hosoya, and D. M. de Leeuw, Phys. Rev. B **44**, 4570 (1991).
[35]S. Smadici, J. C. T. Lee, S. Wang, P. Abbamonte, G. Logvenov, A. Gozar, C. Deville Cavellin, and I. Bozovic, Phys. Rev. Lett. **102**, 107004 (2009).
[36]S. Eisebitt, T. Boske, J.-E. Rubensson, and W. Eberhardt, Phys. Rev. B **47**, 14103 (1993).
[37]P. Kuiper, J. van Elp, D. E. Rice, D. J. Buttrey, H.-J. Lin, and C. T. Chen, Phys. Rev. B **57**, 1552 (1998).
[38]Y. Guo, J.-M. Langlois, and W. A. Goddard III, Science **239**, 896 (1988).
[39]R. Liang, D. A. Bonn, and W. N. Hardy, Phys. Rev. B **73**, 180505(R) (2006).
[40]D. G. Hawthorn, K. M. Shen, J. Geck, D. C. Peets, H. Wadati, J. Okamoto, S.-W. Huang, D. J. Huang, H.-J. Lin, J. D. Denlinger, R. Liang, D. A. Bonn, W. N. Hardy, and G. A. Sawatzky, Phys. Rev. B **84**, 075125 (2011).
[41]P. Abbamonte, L. Venema, A. Rusydi, G. A. Sawatzky, G. Logvenov, and I. Bozovic, Science **297**, 581 (2002).
[42]P. Abbamonte, G. Blumberg, A. Rusydi, A. Gozar, P. G. Evans, T. Siegrist, L. Venema, H. Eisaki, E. D. Isaacs, and G. A. Sawatzky, Nature (London) **431**, 1078 (2004).
[43]P. Abbamonte, A. Rusydi, S. Smadici, G. D. Gu, G. A. Sawatzky, and D. L. Feng, Nat. Phys. **1**, 155 (2005).
[44]S. Smadici, P. Abbamonte, A. Bhattacharya, X. Zhai, B. Jiang, A. Rusydi, J. N. Eckstein, S. D. Bader, and J.-M. Zuo, Phys. Rev. Lett. **99**, 196404 (2007).
[45]S. Smadici, J. C. T. Lee, J. Morales, G. Logvenov, O. Pelleg, I. Bozovic, Y. Zhu, and P. Abbamonte, Phys. Rev. B **84**, 155411 (2011).
[46]K. Nakamura, T. Arima, A. Nakazawa, Y. Wakabayashi, and Y. Murakami, Phys. Rev. B **60**, 2425 (1999).
[47]S. Smadici, J. C. T. Lee, G. Logvenov, I. Bozovic, and P. Abbamonte (unpublished).
[48]N. Nakagawa, H. Y. Hwang, and D. A. Muller, Nat. Mater. **5**, 204 (2006).
[49]B. L. Henke, E. M. Gullikson, and J. C. Davis, At. Data Nucl. Data Tables **54**, 181 (1993).
[50]W. A. Hendrickson, Science **254**, 51 (1991).
[51]I. K. Robinson and D. J. Tweet, Rep. Prog. Phys. **55**, 599 (1992).
[52]V. J. Emery and S. A. Kivelson, Nature (London) **374**, 434 (1995).